A cell-based bioluminescence reporter assay of human Sonic Hedgehog protein autoprocessing to identify inhibitors and activators

Daniel A. Ciulla[1] , Patricia Dranchak[2] , John L. Pezzullo[3] , Rebecca A. Mancusi[1] , Alexandra Maria Psaras[1] , Ganesha Rai[2] , José-Luis Giner[3,*] , James Inglese[2,4,*] , and Brian P. Callahan[1,*]

From the [1]Chemistry Department, Binghamton University, Binghamton, New York, USA; [2]National Center for Advancing Translational Sciences, National Institutes of Health, Rockville, Maryland, USA; [3]State University of New York, College of Environmental Science and Forestry, Syracuse, New York, USA; [4]National Human Genome Research Institute, National Institutes of Health, Bethesda, Maryland, USA

Edited by Ruma Banerjee

The Sonic Hedgehog (SHh) precursor protein undergoes biosynthetic autoprocessing to cleave off and covalently attach cholesterol to the SHh signaling ligand, a vital morphogen and oncogenic effector protein. Autoprocessing is self-catalyzed by SHhC, the SHh precursor's C-terminal enzymatic domain. A method to screen for small molecule regulators of this process may be of therapeutic value. Here, we describe the development and validation of the first cellular reporter to monitor human SHhC autoprocessing noninvasively in high-throughput compatible plates. The assay couples intracellular SHhC autoprocessing using endogenous cholesterol to the extracellular secretion of the bioluminescent nanoluciferase enzyme. We developed a WT SHhC reporter line for evaluating potential autoprocessing inhibitors by concentration response-dependent suppression of extracellular bioluminescence. Additionally, a conditional mutant SHhC (D46A) reporter line was developed for identifying potential autoprocessing activators by a concentration response-dependent gain of extracellular bioluminescence. The D46A mutation removes a conserved general base that is critical for the activation of the cholesterol substrate. Inducibility of the D46A reporter was established using a synthetic sterol, 2-α carboxy cholestanol, designed to bypass the defect through intramolecular general base catalysis. To facilitate direct nanoluciferase detection in the cell culture media of 1536-well plates, we designed a novel anionic phosphonylated coelenterazine, CLZ-2P, as the nanoluciferase substrate. This new reporter system offers a long-awaited resource for small molecule discovery for cancer and for developmental disorders where SHh ligand biosynthesis is dysregulated.

Sonic Hedgehog (SHh) ligands initiate vital cell signaling necessary for brain development and neural stem cell proliferation, while displaying oncogenic activity when dysregulated in sporadic tumors (1–7). The role of SHh signaling in health and disease, particularly in cancer, has prompted efforts to identify clinically useful antagonists of different pathway components (8–12). Many SHh signaling inhibitors target Smoothened (SMO), a cell surface receptor involved in SHh signal transduction (8); however, mutational escape from the antitumor effects of those SMO inhibitors presents a challenge to durable remission (13–15). Thus, new targets to suppress oncogenic SHh ligand signaling are of interest. In a different context, activating the SHh pathway holds promise for developmental disorders where the native function of SHh is compromised by diminished expression. Mutations in the human *SHh* gene are implicated in holoprosencephaly (HPE), a devastating congenital disorder affecting fetal brain development (16). Roughly half of the reported HPE-associated mutations in *SHh* map to the gene's 3′ region (5) encoding a partially characterized autoprocessing domain called SHhC. In this context, small molecules that enhance SHh signaling by restoring SHhC function could find therapeutic application.

The autoprocessing SHhC domain is present in the precursor form of SHh where it self-catalyzes an essential biosynthetic step called cholesterolysis. Cholesterolysis occurs in the endoplasmic reticulum (ER) and results in the release and carboxyl terminal cholesterylation of the adjacent SHh ligand domain (Fig. 1, *left*) (17–19). The native reaction begins with a backbone peptide bond rearrangement at the junction between the SHh ligand and the SHhC domain. This rearrangement activates the terminal Gly residue of the SHh ligand as a thioester at the Cys (C1) side chain of SHhC. Mechanistic overlap exists here with self-splicing inteins (20, 21). In a step unique to Hh family proteins, SHhC then catalyzes nucleophilic attack at the internal thioester by a cholesterol molecule. A conserved aspartate residue of SHhC, Asp46 (D46), is the putative general base for the attacking C3-OH group of cholesterol (22). Cleavage releases cholesterylated SHh ligand for N-palmitoylation, Golgi transport, extracellular secretion, and downstream cell/cell signaling. Mutations that deactivate SHhC result in SHh precursor retention in the ER and eventual removal through ER-associated degradation (ERAD) (23–25). Engineered sterols have the potential to circumvent
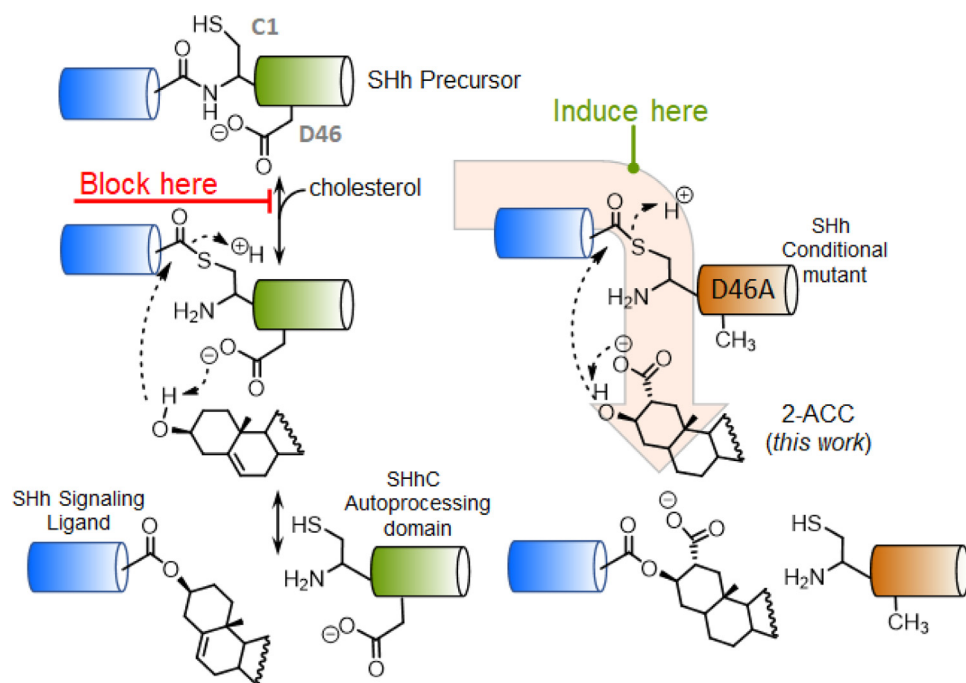
Figure 1. Native Hedgehog SHhC autoprocessing with substrate cholesterol and non-native, induced autoprocessing using chemical rescue approach. *Left*, in the native cholesterolysis pathway, SHhC (*green*) activates then cleaves off the adjacent SHh ligand (*blue*) using cholesterol as the terminal nucleophile. *Right*, defective autoprocessing by SHhC point mutant, D46A (*orange*), is reactivated by engineered sterols, such as 2α carbox-ycholestanol (2-ACC), described here.

catalytic defects in SHhC and restore SHh ligand biosynthesis in some autoprocessing mutants (Fig. 1, *right*) (Ref (26) and this work).

Here, we describe and validate the first homogenous live cell autoprocessing assay to screen for inhibitors and activators of human SHhC function. Chemical activators of SHhC could mitigate the impact of autoprocessing mutations, diminishing HPE pathology; antagonists of SHhC provide a novel means to block oncogenic biosynthesis of the Sonic Hh ligand (13, 27). Our method couples intracellular SHhC autoprocessing to the extracellular secretion of the ATP-independent nanoluciferase (NLuc) enzyme (28). A Sonic Hedgehog WT autoprocessing reporter line is established in HEK293 cells for evaluating SHhC inhibitors by a concentration-dependent loss of extracellular NLuc bioluminescence. We also describe and validate an inducible autoprocessing mutant (D46A) for identifying SHhC activators by the gain of extracellular NLuc bioluminescence. Direct NLuc detection in the media of 1536-well cell culture plates is facilitated by using methylphosphonic acid coelenterazine, CLZ-2P, a novel anionic substrate analog for NLuc.

Results

Reporter strategy

Autoprocessing activity of precursor Sonic Hh protein appears to reside exclusively in SHhC. The SHh ligand is a spectator to the transformation and this arrangement allows for the substitution of the SHh ligand with heterologous polypeptides. Chimeric, functional SHh reporter constructs have been described where GFP is fused to SHhC and more recently, where Halo-Tag is fused to SHhC (29, 30). We substituted the SHh ligand with HA-tagged nanoluciferase (28) (HA-NLuc) with a view toward an high-throughput screening (HTS)–compatible assay system.

Three related HA-NLuc-SHhC fusion constructs were prepared (Fig. 2A). First, a WT HA-NLuc-SHhC was designed for assessment of native SHhC activity and to characterize potential autoprocessing inhibitors. Autoprocessing of the WT reporter construct is expected to cleave off and cholesterylate HA-NLuc using cellular cholesterol in the ER. Cholesterylated HA-NLuc would then transit through the secretory pathway for extracellular release. NLuc activity present in the culture media thereby reports cellular SHhC autoprocessing. The N-terminal HA-tag of NLuc enables the analysis of SHhC autoprocessing by Western blot. The WT reporter construct is intended for evaluating autoprocessing inhibitors by a decrease in extracellular NLuc and by an accumulation of intracellular WT precursor.

We prepared a control construct, C1A, to mimic 100% inhibition of SHhC autoprocessing. This reporter fuses HA-NLuc to a C1A mutant of SHhC. The Cys>Ala mutation at position 1 of SHhC removes the critical nucleophilic thiol group required for thioester formation, thereby blocking SHhC enzymatic function. The precursor form of the C1A reporter is expected to remain largely in the cellular fraction where it would be subject to degradation by ERAD. Compounds that act specifically toward SHhC autoprocessing are not expected to influence bioluminescence from the catalytically inactive C1A or alter the reporter protein's steady-state expression when analyzed by Western blot.
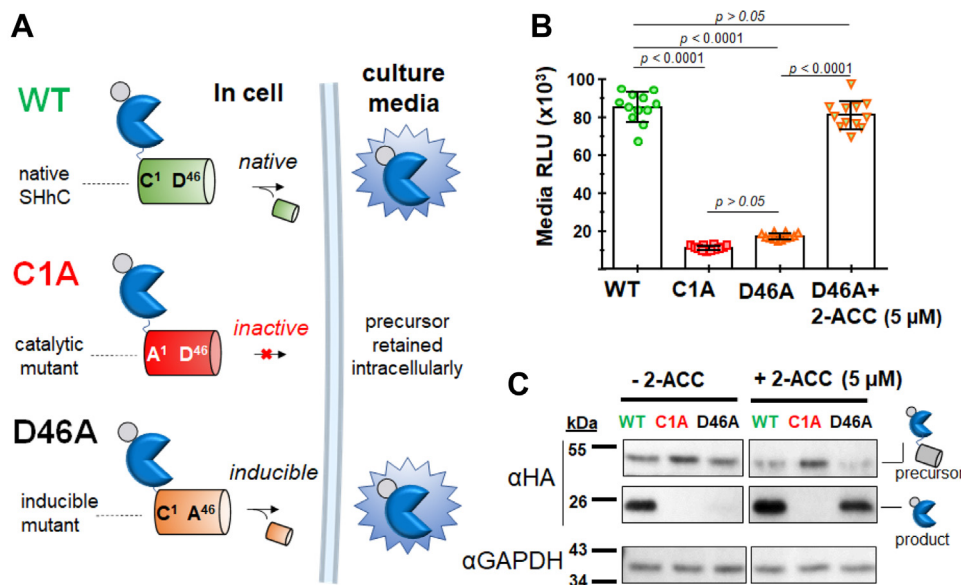
Figure 2. Monitoring autoprocessing in live cells using HA-tagged nanoluciferase (HA-NLuc) as a secreted, proxy reporter of SHhC activity. *A*, autoprocessing reporter constructs. WT, constitutively active autoprocessing using cellular cholesterol; C1A, irreversibly inactive autoprocessing mutant; D46A, conditional mutant with inducible autoprocessing activity. Reporter constructs carry an N-terminal HA epitope tag (*gray*) for Western analysis and the NLuc (*blue*) enzyme for non-invasive measurements of autoprocessing by media bioluminescence. *B*, media bioluminescence reflects intracellular SHhC autoprocessing. Functional behavior of the WT, C1A, and D46A reporters was evaluated 18 h after transient transfection in HEK293 cells (n = 12). Inducibility of the D46A reporter was assessed by comparison of ± the activator, 2-ACC (5 μM). No cholesterol was added above the cholesterol in the 10% FBS present the culture media. Statistical analysis: ANOVA followed by Tukey's pairwise comparison using GraphPad Prism. *C*, Western blot for WT, C1A, and D46A precursor and product using the N-terminal HA epitope. Cell extract from HEK293 cells was analyzed 18 h after transient transfection of the three reporter constructs in the absence (*left*) and presence (*right*) of 2-ACC (5 μM). GAPDH served as a loading control.

In the third construct, we fused HA-NLuc to a D46A point mutant of SHhC for an autoprocessing reporter with inducible activity. The D46A construct is intended for evaluating small molecules as potential autoprocessing activators. Earlier studies on *Drosophila* Hh autoprocessing indicated that D46A mutants of HhC can form internal thioester; however, without the conserved active site D46 carboxylate group, transesterification to substrate cholesterol is prevented (22). The corresponding D46A mutation in human SHhC was expected to behave in a similar manner, blocking native cholesterolysis in cells. Based on our experiments with *Drosophila* HhC, we hypothesized that internal thioester generated by D46A could be resolved with rationally designed analogs such as 3-HPC (3-β hydroperoxycholestane) that can bypass the mutant's catalytic defect (26). For the *in vitro* cell culture work here, we prepared a more chemically stable hypernucleophilic analog, 2-α carboxy cholestanol (2-ACC). The carboxylate group vicinal to the attacking C3 hydroxyl group in 2-ACC was designed to functionally replace the missing carboxylate in the D46A mutant (Fig. 1, *right*; and Fig. 3). Later, we demonstrate that 2-ACC serves as an intracellular inducer of D46A.

NLuc as a surrogate SHhN ligand and extracellular bioluminescent reporter

Initial characterization of the SHhC autoprocessing reporters was carried out by transient transfection using HEK293 cells. HEK293 have been used before for cellular studies of human SHhC autoprocessing (31, 32). The WT, C1A, and D46A chimeric precursors were cloned into the pDisplay (Invitrogen) mammalian expression vector in frame

with the vector's N-terminal Ig κ-chain secretion sequence and HA epitope tag. Following transfection in HEK293, SHhC activity was assayed by NLuc bioluminescence in the culture media and by Western blot of the cell extract.

Figure 2B summarizes media bioluminescence using the NLuc NanoGlo reagent (Promega) following transient transfections with the three reporter plasmids. Samples were collected and analyzed 18 h after transfection. The first column in Figure 2B (*green circles*) shows readings from the WT
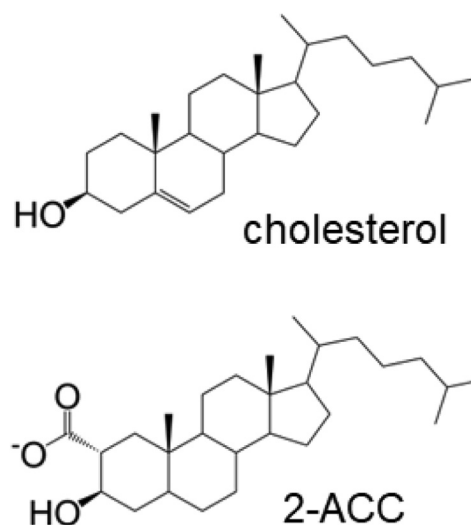

Figure 3. Substrate cholesterol for WT reporter autoprocessing and synthetic activator substrate, 2-ACC, for inducing autoprocessing by the D46A reporter.

samples. The mean bioluminescence value for the WT transfected cells was consistently the highest of the four conditions tested here, in accord with fully active SHhC autoprocessing. The catalytic mutant, C1A (Fig. 2B, *red squares*) by contrast had the lowest output, reduced from WT by 6.5-fold, consistent with defective autoprocessing and intracellular precursor retention (23).

The last two columns in Figure 2B show the media bioluminescence from HEK293 cells transfected with the D46A reporter plasmid (−) and (+) 2-ACC (5 μM). In samples lacking 2-ACC, the D46A samples produced media bioluminescence that is on par with the C1A reporter. This correspondence is consistent with the inability of D46A to autoprocess using cellular cholesterol. The last column in Figure 2B showing D46A (+) 2-ACC indicates a clear gain of media bioluminescence (4.6-fold) relative to D46A without 2-ACC. The enhanced signal is exciting and supports the induction of autoprocessing in HEK293 cells by added 2-ACC. Examples like this where "chemical rescue" of a mutant enzyme that occurs in the cell are rare (33–35). Induced cellular autoprocessing of D46A by 2-ACC is further supported by Western blot analysis, described next. In the SI material, we also report that the corresponding D46A mutant of *Drosophila* HhC has its defective autoprocessing activity restored by 2-ACC (Fig. S1). Bioluminescence was not appreciably enhanced when 2-ACC was added to cells transfected with the C1A or WT reporters, consistent with the specificity of this induction. Overall, the results of the transient transfection experiments in Figure 2B provide proof of concept for the WT, C1A, and D46A reporters.

To complement the comparison based on NLuc bioluminescence, we probed the corresponding cellular fractions of WT, C1A, and D46A by Western blot using the construct's HA epitope tag (Fig. 2C). Lysate samples were denatured, separated by SDS-PAGE, and probed with a monoclonal HA-horseradish peroxidase (HRP) antibody (Sigma) to identify precursor protein, HA-NLuc-SHhC (52 kDa), and autoprocessing product, HA-NLuc (24.4 kDa). Analysis of samples with the WT reporter confirmed SHhC autoprocessing activity, with precursor and product in a ratio of ∼1 to 10. Lysate from the C1A samples showed signal for precursor only, consistent with deactivated SHhC autoprocessing. In D46A, induction of autoprocessing was evident by comparison of samples (−)/(+) 2-ACC. In the absence of 2-ACC, the D46A precursor is expressed without appreciable generation of autoprocessing product. By contrast, signal for the D46A precursor decreases in the (+) 2-ACC sample and the HA-NLuc product signal accumulates, consistent with restored SHhC autoprocessing. The D46A induction was shown to be specific to 2-ACC (Fig. 2C, compare −/+ 2-ACC sample sets for D46A with WT and C1A and *vide infra*).

Miniaturizing the NLuc-SHhC autoprocessing reporter system for 1536-well plates

With a view toward applications to high-throughput chemical screening for inhibitors and activators (36) of SHhC, we sought to streamline assay setup by first preparing stable WT and D46A reporter cell lines. CRISPR/Cas9–targeted gene insertion (37) was used to integrate the two reporter constructs into HEK293 cells (Experimental procedures).

In line with the transient transfection results aforementioned, the stable WT line showed constitutive autoprocessing with strong bioluminescence output in the culture media. We found that treatment of the WT line with brefeldin A, a protein secretion blocker that disrupts ER to Golgi transport, attenuated media bioluminescence, supporting the notion that NLuc activity in the media largely reflects secretory pathway transport rather than non-specific cell leakage (Fig. 4A). Bioluminescence in the lysate fraction remained relatively constant, indicating sustained expression of the WT construct in brefeldin A–treated cells (Fig. 4A, inset). For additional validation, we tested whether the WT reporter would recapitulate the ERAD/proteasome sensitivity observed with native human Sonic Hh precursor (23). Studies by Salic *et al.* suggest that the human SHh precursor in the ER is subjected to a dynamic partitioning between native autoprocessing and ERAD-mediated proteasome degradation. We monitored WT precursor levels by Western blot following various treatments. We first treated the WT line with the protein synthesis inhibitor cycloheximide (CHX). With CHX, we observed a time-dependent precursor loss (Fig. 4B, CHX, top row of Western blot), which could be attributed to native autoprocessing as well as to ERAD. For comparison, in the untreated (dimethyl sulfoxide [DMSO] only) samples, the HA-NLuc-SHhC precursor appears to be at a steady state (Fig. 4B, no treatment). To separate the influence of native autoprocessing from ERAD degradation, the WT line was treated initially with the proteasome inhibitor MG132. Inhibiting the proteasome resulted in a ∼70% increase in the precursor signal. Precursor accumulation is consistent with diminished ERAD (Fig. 4B, MG132). Next, the WT cells were treated with a combination of CHX and MG132. Here, we observed a more gradual consumption of precursor (Fig. 4B, MG132+CHX). Under this final condition, precursor levels should predominantly reflect SHhC autoprocessing with endogenous cholesterol (23). Overall, the pattern of accumulation and depletion of the WT precursor protein in Figure 4B agrees with the dynamic partitioning between ERAD-mediated destruction and SHhC autoprocessing observed with native SHh precursor.

The stable HEK293 D46A reporter line displayed specific, 2-ACC inducible autoprocessing activity as measured by extracellular NLuc activity and in accord with the transient transfection experiments. In the absence of 2-ACC, the D46A reporter line again displayed low media bioluminescence, consistent with intracellular retention. As shown in Figure 5A, there was a gain of media bioluminescence with added 2-ACC that was concentration-dependent and saturable over an 11-pt titration, from 20 nM to 20 μM in 2-ACC. Analysis of the concentration-response data by nonlinear regression yielded an EC_{50} value of 1.6 μM for 2-ACC. As an additional control, we added cholesterol to the D46A line at a concentration equivalent to 2-ACC (5 μM); no increase in media
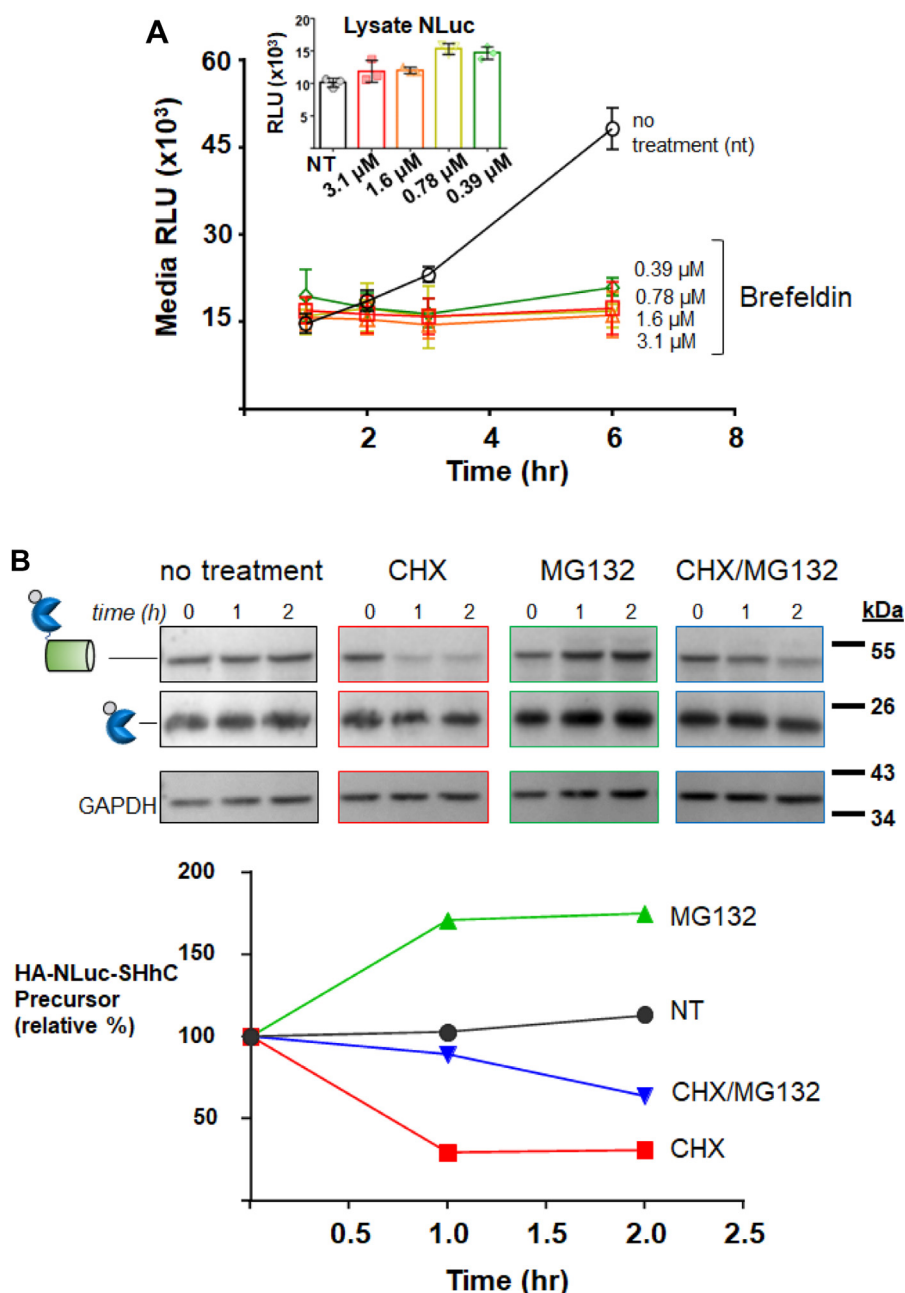
Figure 4. Validation of the WT line as a reporter for native SHhC autoprocessing. *A*, extracellular secretion of NLuc by WT reporter blocked by Brefeldin A. Media bioluminescence was measured 1, 2, 3, and 6 h after addition of the indicated concentrations of Brefeldin A. (inset) Bioluminescence from samples of the corresponding cell lysate fraction after 6 h Brefeldin A treatment. *B*, intracellular WT reporter protein response to cycloheximide (CHX) and MG132. *Upper*, Western blot analysis. Control samples treated with DMSO control; 25 µg/ml cycloheximide; 50 µM MG132; and cotreated with 25 µg/ml CHX and 50 µM MG132. *Lower*, plot of WT precursor abundance using Western blot images shown based on analysis with Image J. DMSO, dimethyl sulfoxide.

bioluminescence was apparent (Fig. 5B). The hyper-nucleophilic 3-HPC failed to produce measurable induction of cellular autoprocessing by D46A, likely a consequence of the hydroperoxide groups instability.

Next, we focused on optimizing and miniaturizing the WT/D46A reporter system to the 1536-well format. To streamline the assay, we designed and synthesized the anionic coelenterazine analog (CLZ-2P) (Fig. 6A). Traditional imidazopyrazinone nanoluciferase substrates such as coelenterazine (CLZ-H) and furimazine (NanoGlo) are uncharged and membrane permeable and therefore require careful media

transfer from the cell culture plate to an assay plate to separate signal from intracellular and extracellular NLuc (38). Intracellular NLuc could include product and precursor forms of the SHhC reporter proteins used here, confounding analysis of autoprocessing activity; whereas extracellular NLuc is expected to reflect autoprocessing product only. CLZ-2P, incorporating the anionic methylphosphonic acid at the 2-(4-hydroxybenzyl) moiety of CLZ-H was devised to eliminate cell permeability and the media transfer step for measurement of media bioluminescence. The C-P phosphonyl bond in CLZ-2P stabilizes the anionic group against P-O cleaving
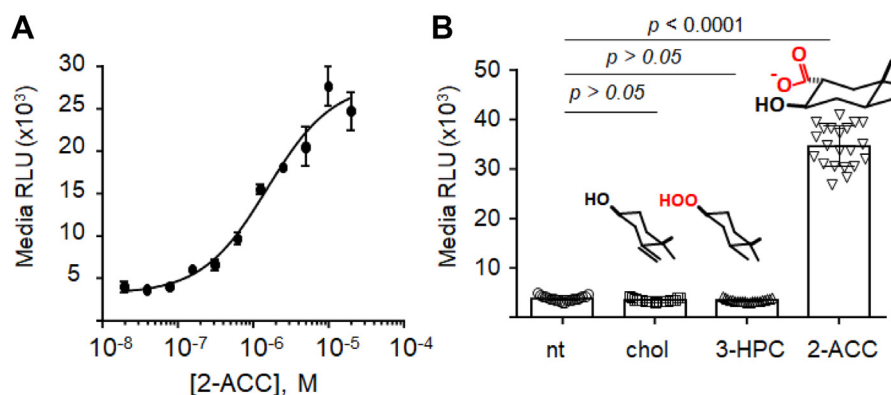
Figure 5. Validation of the D46A line as a chemically inducible SHhC autoprocessing reporter. *A*, concentration-response activation curve for 2-ACC based on media NLuc activity from D46A (*n = 4*). EC_{50} = 1.6 μM. *B*, induced autoprocessing with D46A is 2-ACC specific. Endogenous cholesterol supplied by the 10% FBS—no additional cholesterol added (no treatment); additional cholesterol added (5 μM, final), added 3-HPC (5 μM, final) compared with added 2-ACC (5 μM, final) as potential inducers of D46A autoprocessing (n = 21). Statistical analysis: ANOVA, Tukey's pairwise comparison (GraphPad Prism). FBS, fetal bovine serum.

phosphatases, similar to the previously described analog described by Lindberg *et al.* (39), but synthetically more tractable for quantities needed in HTS applications. The data in Figures 6B, 7 and S4 supports CLZ-2P as an alternative NLuc substrate that is suited for mix-and-read assays of the WT and D46A in 1536-well plates.

Analysis of the WT and D46A reporter lines in the 1536-well plate format was conducted hereafter using CLZ-2P. We observed a relatively low coefficient of variation of 4% to 5% between 32 intraplate replicates for both cell lines (Table S1), demonstrating well-to-well reproducibility in this assay format. Both reporter lines yielded a suitable Z′ factor, with WT = 0.83 and D46A = 0.64, using CHX and 2-ACC, respectively (36). In Figure 7, *A* and *B*, the concentration-response curves are shown for D46A and WT treated with 2-ACC and CHX. In agreement with the experiments aforementioned, activation by 2-ACC is specific to D46A, with an EC_{50} of ~5 μM and ~100% activation at 28.75 μM 2-ACC. Extracellular secretion of NLuc by WT was also shown to be sensitive to CHX treatment, with maximum inhibition of NLuc activity in the media at 57.5 μM CHX. As an additional test, cells were treated with the membrane-disrupting digitonin toxin and cytotoxicity was measured with CellTiter-Glo assay reagent. D46A and WT responded near identically, with maximum lethal digitonin concentration of 115 μM, Z′ factor = 0.87 (Fig. 7C). Taken together, the robust performance of the two stable lines in HTS-compatible plates, along with the efficacy of CLZ-2P as an NLuc substrate for media bioluminescence measurements, encourage the application of this novel reporter system to identify the first chemical probes of SHhC autoprocessing.

Discussion

Early biochemical studies on chicken SHh protein demonstrated "proteolytic processing" into two SHh products of approximately 19 kDa (SHh ligand) and 27 kDa (SHhC) (17). Work carried out around the same time with mouse SHh reported similar behavior (40). Both studies involved transient expression of the full-length SHh precursor in cultured eukaryotic cells, followed by Western blotting of cell lysate. Gel-based assays remain the standard approach to monitor cellular SHh autoprocessing, despite the method's idiosyncrasies, expense, and low throughput. Cell-free and gel-free autoprocessing assays using recombinant protein, which we recently devised for kinetic studies of *Drosophila* Hh autoprocessing (41, 42), have so far resisted application to the human Hh homologs. In our hands, only sparing amounts of bacterially expressed human SHhC can be recovered and that material seems to lack autoprocessing activity. Requirements for N-linked glycosylation (24) and reductive activation (23) of SHhC in the mammalian ER offer a possible explanation.

The *in vitro* live cell SHhC activity assay reported here represents an important resource for future studies of human Hh protein autoprocessing. With NLuc as the surrogate SHh ligand, intracellular SHhC autoprocessing is coupled to the secretion of a thermostable, ATP-independent bioluminescent reporter. Measurement of NLuc enzymatic activity is carried out noninvasively in a semiquantitative manner in culture media. We show that bioluminescent output is sufficiently robust for miniaturization to 1536-well plates. Inhibitors of SHhC autoprocessing are expected to suppress NLuc secretion from cells expressing the WT reporter, while activators of SHhC autoprocessing are identified by enhanced NLuc secretion from the D46A reporter. The development of CLZ-2P as an impermeable substrate for NLuc increases assay throughput. With CLZ-2P, measurements of secreted NLuc are completed as a simple mix-and-read step in the presence of live cells.[†]

[†] A modified version of the FRET-based biochemical reporter of HhC autoprocessing (Ref (42)) was considered initially for the purpose of monitoring intracellular human SHhC autoprocessing. We elected to pursue bioluminescence from NLuc instead of using a FRET reporter for several reasons: the greater sensitivity possible with the enzyme amplified output signal from NLuc; the smaller size of NLuc (19 kDa) compared to a FRET-active pair of fluorescent proteins (60 kDa); and the expectation of a more straightforward means of signal measurement and greater dynamic range of that signal with the NLuc reporter compared with a ratiometric FRET reporter.
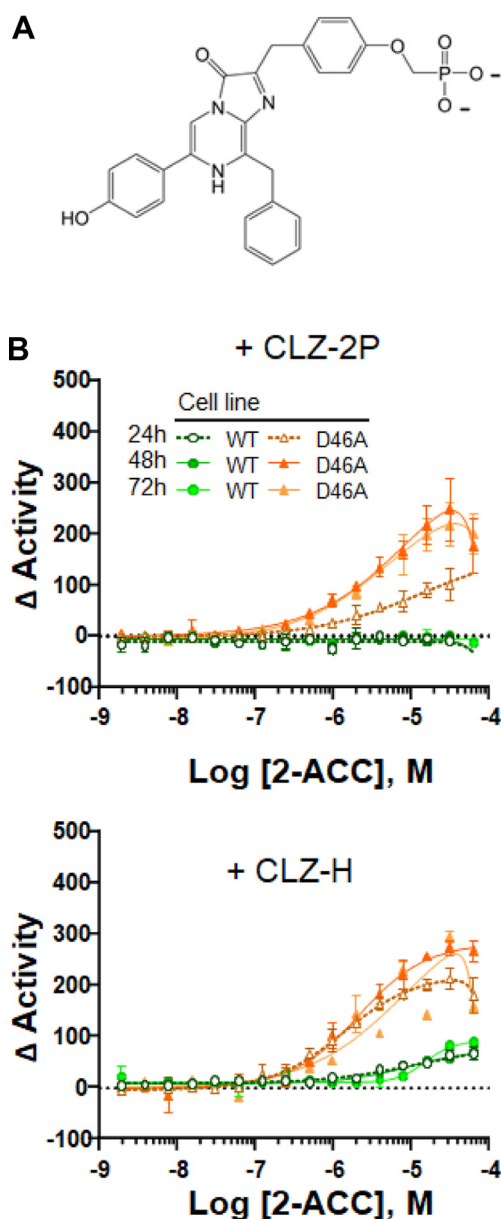
A

B

Figure 6. Validation of CLZ-2P for mix-and-read measurements of extracellular NLuc activity. *A*, anionic coelenterazine, CLZ-2P. *B*, samples of WT and D46A with added CLZ-2P (*top*) or coelenterazine (CLZ-H) (*bottom*) were analyzed as a function of increasing 2-ACC in 1536-well plates. Data were row-wise normalized to DMSO neutral control at each time point. Error bars represent SD of the average of two replicate wells. DMSO, dimethyl sulfoxide.

The WT and D46A reporter cell lines are poised for quantitative HTS (qHTS) (43) to support the search for chemical probes of this key initiating step in the Sonic Hh signaling pathway. Autoprocessing events like Hh protein cholesterolysis that are single turnover and partly unimolecular represent challenging but not untenable targets for small molecules (42, 44–47). Antagonists of SHhC autoprocessing are sought to inhibit Sonic Hh biosynthesis, blocking the ligand from oncogenic signaling in sporadic tumors. In developmental disorders like HPE where SHh

ligand biosynthesis is compromised by congenital mutation, activators of SHhC could serve as chemical chaperones to restore SHh signaling.

Experimental procedures

Biochemicals and cell biology reagents

DNA restriction enzymes, T4 DNA ligase, and chemically competent DH5 alpha cells (NEB); Alt-R CRISPR-Cas9 crRNA, Cas9 expression plasmid, and PCR oligos (IDT). HA-HRP primary antibody; GAPDH-HRP primary antibody (Santa Cruz SC-365062); Hyclone 0.25% Trypsin-EDTA (GE Life Sciences); penicillin/streptomycin, Eagle's minimum essential medium (EMEM), fetal bovine serum (FBS) (Corning); G418, OptiMEM I (Gibco); digitonin, MG132, CHX (Millipore Sigma); HEK293 cells (ATCC, provided by Tracy Brooks, SUNY Binghamton). Plates: 96-well black polystyrene microplate (Corning 3650), 12-well nunclon delta surface (Thermo Scientific), 96-well tissue culture plate (VWR 734-2327), 50 ml tissue culture flask blue vented cap (Corning 353108), white solid bottom TC treated 1536-well plate (Greiner Bio-One 789173-F).

Reporter constructs

Chimeric SHh precursor encoding HA-tagged NLuc fused to native and mutant forms of human Sonic HhC autoprocessing domain were assembled in pDisplay (Invitrogen). Fragments encoding Sonic HhC were inserted into pDisplay using PstI and XhoI; codon optimized NLuc was inserted using the vector's BglII and PstI sites. An oligo cassette for CRISPR-Cas9 genomic integration was introduced into the vector at a unique SnaBI site. Plasmids were purified for transfection with the ZymoPURE II plasmid midiprep kit (Zymoresearch). We thank Dr Erich Roessler (NIH) for providing a Sonic Hh complementary DNA plasmid. Fig. S2 shows the amino acid sequence of assembled WT chimeric construct.

Transient transfection

HEK293 cells were seeded into a 12-well plate at 100,000 cell/ml in complete EMEM supplemented with 10% FBS and 0.1 % Pen/Strep. When cells reached 70% confluency, media was replaced with reduced serum Opti-MEM I containing lipofectamine-2000 with 1.6 µg/well reporter plasmid. After a 1 h transfection, media was replaced with complete EMEM and the cells were incubated overnight. Cells and media were then collected for bioluminescence assays and Western blot analysis.

HEK293 stable cell line generation using CRISPR/CAS9

We followed the general method outlined by He *et al.*(37) to generate WT and D46A reporter lines. Nucleic acid fragments used for CRISPR/CAS9 integration are found in Fig. S3. HEK293 cells were cultured at 37 °C 5%
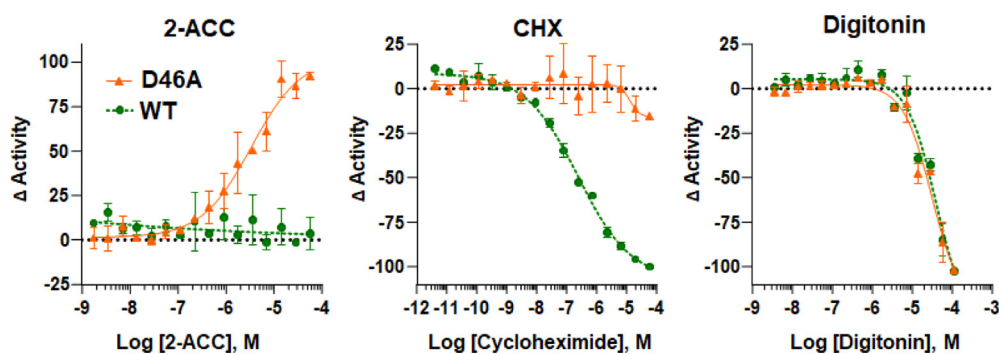
Figure 7. Concentration-response curves for WT and D46A in 1536-well plates with control compounds. Graphs for 2-ACC (*left*) and cycloheximide (*middle*) titrations are based on NLuc bioluminescence in the media using CLZ-2P as NLuc substrate. Digitonin experiments (*right*) are based on cytotoxicity, measured by the CellTiter-Glo reagent. Curves were fit in GraphPad Prism and error bars represent the SD of two replicate wells for each concentration across the respective assay plates. n = 2.

CO_2 in EMEM supplemented with 10% FBS and 0.1% Pen/Strep. Cells were grown to 70% confluency in a 12-well plate. The media was replaced with reduced serum Opti-MEM I containing lipofectamine-2000 (Invitrogen), the pDisplay reporter plasmid (0.6 μg), Cas9 expression plasmid (0.6 μg), and short guide RNA (0.4 μg). After 1 h, the transfection media was replaced with complete media. Following an overnight recovery in complete EMEM, the media was exchanged with complete EMEM containing G418 antibiotic (400 μg/ml). Media was then replaced every 2 to 3 days and cells were passaged weekly. Bioluminescence measurements were made periodically to confirm expression of the reporter constructs. After 4 weeks under G418 selection, cells were diluted into 96-well plates at single cell per well density and then expanded into stable cell lines.

Cell lysis and Western blot analysis

HEK293 cells transfected with WT, C1A, or D46A reporter plasmids were lysed after media aspiration by 250 μl ice-cold radioimmunoprecipitation assay buffer (Thermo Scientific). After agitation by orbital shaking for 20 min at room temperature (RT), the lysate suspension was collected into microcentrifuge tubes, treated with DNAse I (12 ng/μl) on ice for 10 min, followed by centrifugation at 18,000*g* for 5 min at 4 °C. The supernatant was transferred to a clean tube and used immediately or stored at –80 °C. For Western analysis, aliquots of the soluble lysate were denatured by boiling at 95 °C for 5 min in SDS-PAGE load buffer (final concentration, bromophenol blue 0.1%, glycerol 10%, SDS 2%, DTT 100 mM, Tris–HCl 50 mM). Denatured proteins were resolved by 12% SDS-PAGE. Following electrophoresis, the gel was submerged for 20 min in transfer buffer (Tris 2.5 mM, glycine 19 mM, 20% methanol, pH 8.3) then electroblotted (20 V) overnight at 4 °C onto a 0.2 μm polyvinylidene difluoride membrane (Amersham Hybond). Following transfer, the membrane was blocked with 5% BLOT-Quick at RT with gentle shaking for 1 h. After rinses with TBST buffer (Tris 2 mM, NaCl 15 mM, Tween-20 0.1%), a solution of TBST/5% BLOT-quick with αHA-HRP (1/500) or αGAPDH-HRP (1/1000) was added. After gentle shaking at 4 °C, overnight, the membrane was rinsed 3× with TBST buffer, followed by a 15 min wash, and then three 5 min washes with TBST buffer. Visualization of HRP was accomplished by colorimetric detection (Femto-Chromo HRP kit, G-Biosciences).

Extracellular NLuc assay for induced autoprocessing in the D46A line

Stable D46A cells were seeded into 96-well plates at a density of 2×10^4 cells/well (total volume 100 μl) and grown to ~70% confluency over 72 h. Seeding media contained 2-ACC, cholesterol, or 3-HPC, titrated over an 11-point 1:2 dilution from 20 μM to 20 nM. At least four intraplate replicates were included for each concentration of sterol. We assayed 10 μl of the media for bioluminescence using the NanoGlo detection reagent (furimazine). We first prepared a NLuc reaction stock solution by combining 980 μl NanoGlo buffer with 20 μl of furimazine substrate. This solution was incubated in the dark at RT for 5 min. During this period, we prepared the bioluminescence assay plate. Each sample well in the assay plate (Corning 3650) contained 90 μl of distilled water and 10 μl media from the cell culture plate. To initiate bioluminescence, 10 μl of the NanoGlo reaction solution was added to each sample well in the assay plate, incubated with gentle shaking for 2 min, and then assayed for bioluminescence using a Biotek Synergy H1 plate reader with gain equal to 150.

Assay miniaturization and NLuc substrate optimization

HEK293 cells expressing WT HA-NLuc-SHhC (WT) and HA-NLuc-SHhC (D46A) were grown in EMEM (ATCC) supplemented with 10% FBS (HyClone), 100 U/ml penicillin, and 100 μg/ml streptomycin (Gibco) in the absence of selection antibiotics. Cells were trypsinized from culture flasks, counted, diluted in growth media, and plated at 1000, 1500, or 2000 cells per 4 μl per well in respective columns of white, solid bottom TC treated 1536-well plates (Greiner Bio-One) with a multidrop combi dispenser (ThermoFisher). Control compound digitonin was prepared at 20 mM stock

concentration in DMSO and diluted in a 16-pt, 1:2 dilution, while MG132 and CHX were prepared at a stock concentration of 10 mM in DMSO and titrated in 16-pt, 1:3 dilution. Each compound titration was transferred in duplicate to respective columns of assay plates along with replicate columns of DMSO vehicle control to seeded cells at 25 nl per well with a mosquito liquid handler (SPTLabTech) immediately after cells were plated. Cells were covered with weighted metal lids with gas exchange pores (Wako) and incubated at 37 °C, 5% CO_2, and 95% humidity. After 24 h, 1 µl media was manually transferred from each well of one assay plate to a recipient white, solid bottom TC treated 1536-well plate with 3 µl 1× PBS predispensed in each well. NanoGlo luciferase assay substrate was prepared at a 1:100 dilution according to manufacturer's protocol and 3 µl NanoGlo substrate was added to each well of media transfer plate and cell source plate with a BioRAPTR FRD (Beckman Coulter). Nanoluciferase luminescence for each plate was read on a ViewLux plate reader (PerkinElmer) after 5 min. Coelenterazine-H substrate was prepared as a 2 mM stock solution in 100% ethanol and coelenterazine-2P was diluted to a 2 mM stock solution in DMSO. Both substrates were prepared in a nonlytic PBS assay buffer (300 mM sodium ascorbate, 5 mM NaCl) at a working dilution of 20 µM. Coelenterazine substrates were added at 4 µl/well to one cellular assay plate each with a BioRAPTR FRD and nanoluciferase luminescence was read on a ViewLux plate reader within 2 to 5 min.

qHTS 2-ACC time course concentration-response validation

Stable HEK293 WT and D46A cells were grown and plated at 1.5×10^3 cells/well (4 µl) in respective columns of six replicate white, solid bottom TC treated 1536-well plates as before. 2-ACC was diluted in a 16-pt, 1:2 dilution starting at a high concentration of 10 mM and was added to the plated cells as aforementioned. Cells were incubated at 37 °C, 5% CO_2, and 95% humidity for 24 to 72 h. Using the mosquito liquid handler, 300 nl of media was transferred from each well of two assay plates to respective white, solid bottom TC treated 1536-well recipient plates containing 4 µl/well 1× PBS every 24 h. One media transfer plate received 3 µl/well NanoGlo substrate while the corresponding cell source plate received 4 µl/well coelenterazine-2P substrate. Luminescence was read on a ViewLux plate reader after a 5 min incubation. Coelenterazine-H was added at 4 µl/well to the second set of plates and luminescence was read after 5 min.

qHTS data analysis

Assay statistics were calculated for 32 replicate wells of DMSO vehicle control and two wells of high concentration of respective compound treatment for initial assay optimization across the cell lines, cell densities, and for each substrate across a 72 h time course. Statistics were then calculated for 64 wells of DMSO vehicle control and 32 replicate wells of max concentration of the respective control compounds for optimal assay conditions of 1500 cells/well treated for 48 h .

Concentration response curves were determined for each compound and data were normalized to DMSO neutral control for each cell density for each cell line. Concentration response curves were fit and EC_{50} values calculated in Prism 7.0 (GraphPad) with nonlinear regression log(agonist) *versus* response–variable slope (four parameters) fit. Bell-shaped curves were also fit in Prism 7.0 with nonlinear regression and the equation:

$$Y = S0 + \frac{(S1-S0)}{\left(1 + 10^{((logEC50-X)\times Hill\ Slope\ 1)}\right)} + \frac{(S2-S1)}{\left(1 + 10^{((logEC50-X)\times Hill\ Slope\ 2)}\right)}$$

2-ACC synthesis
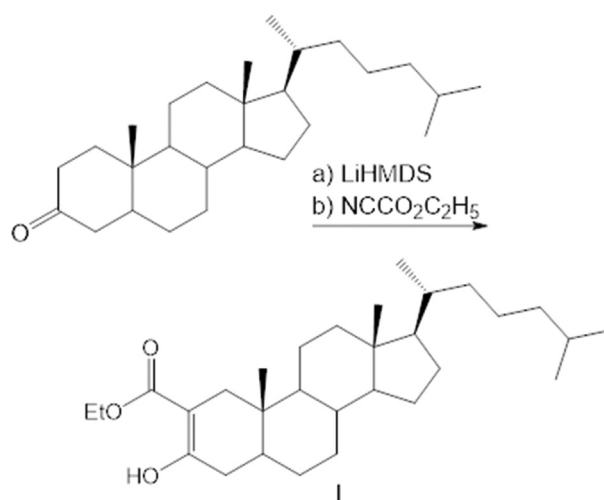
2a-Ethoxycarbonylcholestan-3-one (I)

To a solution of cholestan-3-one (750 mg, 1.95 mmol) in dry THF (10 ml) under N_2 at −78 °C was added 3 ml of LiHMDS (1M in hexane, 3.0 mmol) with stirring over 2 min. After another 20 min, ethyl cyanoformate (0.4 ml, 5.0 mmol) was added and the flask was removed from the bath and allowed to warm to RT. After 3 h, the contents were poured into 150 ml of saturated aqueous $NaHCO_3$ and extracted three times with 40 ml of hexane/EtOAc 9:1. The combined organic phase was washed with 10% hydrochloric acid, brine, dried (Na_2SO_4), and evaporated under reduced pressure. Silica gel column chromatography (hexane/EtOAc 79:1) yielded the product as the enol tautomer (620 mg, 1.36 mmol, 70%). ^{1}H NMR (600 MHz, $CDCl_3$): 12.171 (1H, s), 4.26 to 4.15 (2H, m), 2.297 (1H, d, *J* = 15.6 Hz), 2.121 (1H, dd, *J* = 5.6, 18.8 Hz), 2.04 to 1.96 (2H, m), 1.82 (1H, m), 1.776 (1H, d, *J* = 15.6 Hz), 1.677 (1H, dq, *J* = 2.6, 12.9 Hz), 1.61 to 1.32 (m), 1.299 (3H, t, *J* = 7.1 Hz), 1.28 to 0.94 (m), 0.909 (3H, d, *J* = 6.4 Hz), 0.864 (6H, dd, *J* = 1.8, 6.5 Hz), 0.744 (3H, s), 0.668 (3H, s).
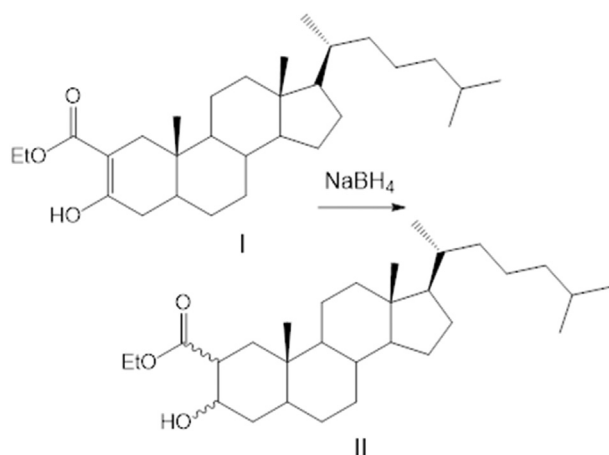
2α-Ethoxycarbonylcholestan-3-ol (II)

To a solution of **I** (51.5 mg, 0.11 mmol) in MeOH/DCM 2:1 (3 ml) was added NaBH$_4$ (29 mg, 0.76 mmol) in one portion. After 45 min, 10% hydrochloric acid (6 ml) was added and the mixture was extracted thoroughly with hexane/EtOAc 4:1. The extracts were filtered through silica gel and evaporated under reduced pressure. Purification *via* preparative TLC (250 μm silica plate, 4:1 hexane/ethyl acetate) yielded **IIa** and **IIb** as an inseparable mixture along with **IIc** as a pure compound. The diastereomers were identified using the NMR shifts of the angular methyl groups and the coupling constants of H-2 and H-3. ^{1}H NMR (600 MHz, CDCl$_3$), **IIa** (2α,3α), 27%: 4.206 (1H, tt, *J* = 2.3, 2.9 Hz), 3.251 (1H, br s), 2.544 (1H, ddd, *J* = 2.5, 3.8, 13.4 Hz), 0.816 (3H, s), 0.654 (3H, s). **IIb** (2β,3β), 49%: 3.592 (1H, tt, *J* = 4.9, 11.9 Hz), 2.383 (1H, dd, *J* = 2.2, 13.9 Hz), 0.715 (3H, s), 0.639 (3H, s). **IIc** (2α,3β), 24%: 3.805 (1H, td, *J* = 4.9, 10.6 Hz), 2.720 (1H, br s), 2.450 (1H, ddd, *J* = 3.9, 10.6, 13.1 Hz), 0.846 (3H, s), 0.647 (3H, s).
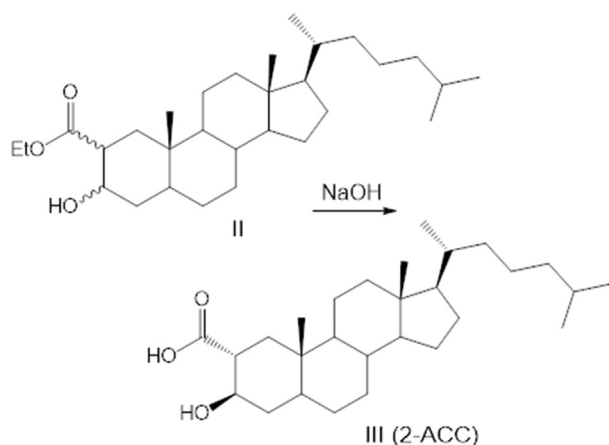
### 3β-Hydroxycholestane-2α-carboxylic acid (III)

To a solution of **IIa/b** (22.0 mg mixed isomers, 0.048 mmol) in DCM (0.5 ml) was added 10% NaOH/MeOH (2.5 ml) and the solution was heated under reflux for 16 h. After cooling to RT, 10% hydrochloric acid (5 ml) was added, the mixture was extracted thoroughly with EtOAc, and the extracts were filtered through Na$_2$SO$_4$. Evaporation under reduced pressure yielded the product (20.6 mg, 100%). The diastereomers were separated by preparative TLC (250 μm silica plate, hexane/EtOAc 1:2 + 5% AcOH) and eluted with 2% AcOH/EtOAc. The more polar band contained the desired product. The procedure was repeated with compound **IIc** to yield an identical sample of **III, 2-ACC**. ^{1}H NMR (800 MHz, CDCl$_3$): 3.818 (1H, td, *J* = 4.7, 10.6 Hz), 2.513 (1H, td, *J* = 3.0, 11.9 Hz), 2.048 (1H, dd, *J* = 3.2, 13.8 Hz), 1.965 (1H, dt, *J* = 3.0, 12.7 Hz), 1.809 (1H, m), 1.658 (2H, m), 1.58 to 1.47 (3H, m), 1.44 to 0.94 (m), 0.896 (3H, d, *J* = 6.4 Hz), 0.862 (6H, dd, *J* = 3.7, 6.6 Hz), 0.855 (3H, s), 0.673 (1H, td, *J* = 3.6, 11.4 Hz), 0.650 (3H, s). ^{13}C NMR (201 MHz): 179.57, 71.14, 56.40, 56.23, 54.03, 46.79, 44.50, 42.55, 40.05, 39.87, 39.51, 36.16, 36.07, 35.78, 35.44, 31.84, 28.26, 28.21, 28.01, 24.18, 23.82, 22.81, 22.55, 21.30, 18.67, 12.52, 12.07. HRMS (HESI) *m/z* [M − H]$^-$: Calcd for C$_{28}$H$_{47}$O$_3$ 431.3525; Found 431.3532 (NMR spectra for I, II, III, see Fig. S5).

CLZ-2-methylphosphonic acid (CLZ-P) synthesis

General methods

All air or moisture-sensitive reactions were performed under a positive pressure of argon with oven-dried glassware. 4M HCl in dioxane and cesium carbonate were purchased from Sigma–Aldrich and used as such. Analytical analysis was performed on an Agilent LC/MS (Agilent Technologies). Method: A 7 min gradient of 4% to 100% acetonitrile (containing 0.025% trifluoroacetic acid [TFA]) in water (containing 0.05% TFA) was used with an 8 min run time at a flow rate of 1 ml/min. A Phenomenex Luna C18 column (3-micron, 3 × 75 mm) was used at a temperature of 50 °C. A Phenomenex Gemini Phenyl column (3-micron, 3 × 100 mm) was used at a temperature of 50 °C. Purity determination was performed using an Agilent Diode Array Detector for both Method 1 and Method 2. Mass determination was performed using an Agilent 6130 mass spectrometer with electrospray ionization in the positive mode. ^{1}H NMR spectra were recorded on Varian 400 MHz spectrometers. Chemical shifts are reported in ppm with undeuterated solvent (DMSO-*d*$_6$ at 2.49 ppm) as an internal standard for DMSO-*d*$_6$ solutions. High-resolution mass spectrometry was recorded on Agilent 6210 Time-of-Flight LC/MS system. Confirmation of molecular formula was accomplished using electrospray ionization in the positive mode with the Agilent Masshunter software (version B.02).

Synthesis of diethyl ((4-(3,3-diethoxy-2-oxopropyl)phenoxy)methyl)phosphonate (3)
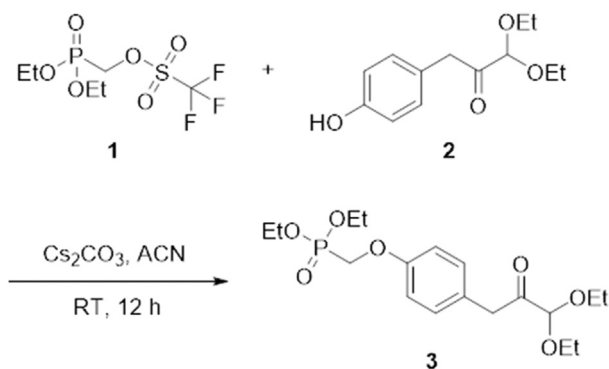
An oven-dried flask containing 1,1-diethoxy-3-(4-hydroxyphenyl)propan-2-one (0.794 g, 3.33 mmol, 1 eq) in acetonitrile (10 ml) was added cesium carbonate (1.628 g, 5.00 mmol, 1.5 eq). After stirring for 10 min at RT, (diethoxyphosphonyl)methyl trifluoromethanesulfonate (1 g, 3.33 mmol, 1 eq) was added and stirred at RT overnight. The reaction mixture was filtered through a pad of Celite and washed with ethyl acetate. The filtrate was concentrated, and the residue was directly loaded to a flash 40 g silica column. The crude product was purified on a flash system eluting with 0% to 100% ethyl acetate in hexanes over 32 column volumes to yield 0.62 g (48%) pure product **3** after evaporating and drying process under high vacuum. LCMS retention time = 5.3 min $(M + H)^+$ for $C_{18}H_{30}O_7P$ = 389.2.

Synthesis of CLZ-2-methylphosphonic acid (CLZ-2P), aka NCATS-SM1462
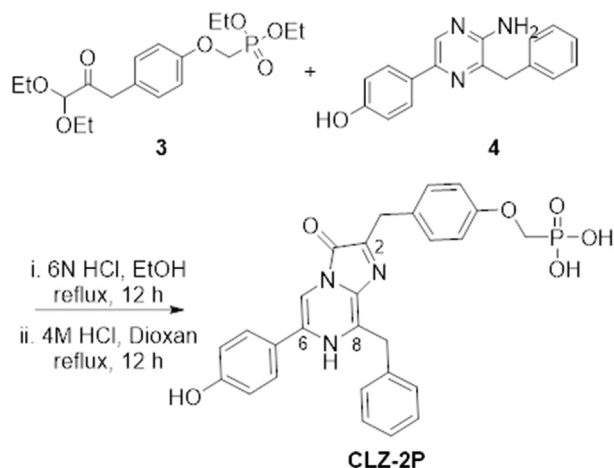
An oven-dried round-bottomed flask containing a mixture of diethyl ((4-(3,3-diethoxy-2-oxopropyl)phenoxy)methyl)

phosphonate 3 (0.617 g, 1.589 mmol, 1.2 eq) and 3-benzyl-5-(4-(2-(trimethylsilyl)ethoxy)phenyl)pyrazin-2-amine 4 (0.5 g, 1.324 mmol, 1 eq; 4 was prepared following the literature method (48)) in degassed ethanol was added 6N HCl (in water) and refluxed overnight. The reaction was concentrated and added 100 ml of 4 M HCl in dioxan and refluxed again overnight at 100 °C to deprotect the ethyl phosphonate groups. The reaction was concentrated on a rotary evaporator and the crude product was purified on a reverse-phase flash system using 120 g C18 column eluting with 5% to 100% acetonitrile (0.1% TFA) in water (0.1% water). The product fraction was pooled and concentrated to obtain the relatively pure product, which was further purified on an HPLC system eluting with water/acetonitrile (modified with 0.1% NH_4OH) using the basic method. A small portion was further subjected to HPLC purification using an acidic method to obtain pure material of yellow CLZ-2P as a TFA salt. LC-MS retention time = 3.54 min $(M + H)^+$ for $C_{27}H_{25}N_3O_6P$ = 518.1.; 1H NMR (400 MHz, dmso) δ 10.90 (brs, 1H), 9.73 (brs, 1H), 7.82 to 7.52 (m, 2H), 7.44 (d, J = 7.5 Hz, 2H), 7.34 to 7.17 (m, 5H), 6.95 to 6.88 (m, 2H), 6.88 to 6.80 (m, 2H), 4.30 (s, 2H), 4.07 to 3.96 (m, 4H); HRMS (ESI) m/z (M + H)+ calcd. for $C_{27}H_{25}N_3O_6P$ = 518.1475, found 518.1560 (NMR spectrum for CLZ-2P, see Fig. S6).

Data availability

Requests for materials and data supporting this study may be addressed to Brian Callahan (callahan@binghamton.edu).

Conflict of interest—The authors declare that they have no conflicts of interest with the contents of this article.

Abbreviations—The abbreviations used are: 2-ACC, 2-α carboxy cholestanol; CHX, cycloheximide; DMSO, dimethyl sulfoxide; EMEM, Eagle's minimum essential medium; ER, endoplasmic reticulum; ERAD, ER-associated degradation; FBS, fetal bovine serum; HPE, holoprosencephaly; HRP, horseradish peroxidase; HTS, high-throughput screening; qHTS, quantitative HTS.

References

1. Rallis, A., Navarro, J. A., Rass, M., Hu, A., Birman, S., Schneuwly, S., *et al.* (2020) Hedgehog signaling modulates glial proteostasis and lifespan. *Cell Rep.* **30**, 2627–2643.e5

2. Lai, K., Kaspar, B. K., Gage, F. H., and Schaffer, D. V. (2003) Sonic Hedgehog regulates adult neural progenitor proliferation *in vitro* and *in vivo*. *Nat. Neurosci.* **6**, 21–27

3. Liu, Z., Xu, J., He, J., Zheng, Y., Li, H., Lu, Y., *et al.* (2014) A critical role of autocrine Sonic Hedgehog signaling in human CD138+ myeloma cell survival and drug resistance. *Blood* **124**, 2061–2071

4. Bissey, P. A., Mathot, P., Guix, C., Jasmin, M., Goddard, I., Costechareyre, C., *et al.* (2020) Blocking SHH/patched interaction triggers tumor growth inhibition through patched-induced apoptosis. *Cancer Res.* **80**, 1970–1980

5. Hong, S., Hu, P., Jang, J. H., Carrington, B., Sood, R., Berger, S. I., *et al.* (2020) Functional analysis of Sonic Hedgehog variants associated with holoprosencephaly in humans using a CRISPR/Cas9 zebrafish model. *Hum. Mutat.* **41**, 2155–2166

6. Roessler, E., El-Jaick, K. B., Dubourg, C., Velez, J. I., Solomon, B. D., Pineda-Alvarez, D. E., *et al.* (2009) The mutational spectrum of holoprosencephaly-associated changes within the SHH gene in humans predicts loss-of-function through either key structural alterations of the ligand or its altered synthesis. *Hum. Mutat.* **30**, E921–E935

7. Chen, M., Tanner, M., Levine, A. C., Levina, E., Ohouo, P., and Buttyan, R. (2009) Androgenic regulation of Hedgehog signaling pathway components in prostate cancer cells. *Cell Cycle* **8**, 149–157

8. Quaglio, D., Infante, P., Di Marcotullio, L., Botta, B., and Mori, M. (2020) Hedgehog signaling pathway inhibitors: an updated patent review (2015-present). *Expert Opin. Ther. Pat.* **30**, 235–250

9. Jamieson, C., Martinelli, G., Papayannidis, C., and Cortes, J. E. (2020) Hedgehog pathway inhibitors: a new therapeutic class for the treatment of acute myeloid leukemia. *Blood Cancer Discov.* **1**, 134–145

10. Petrova, E., Rios-Esteves, J., Ouerfelli, O., Glickman, J. F., and Resh, M. D. (2013) Inhibitors of Hedgehog acyltransferase block Sonic Hedgehog signaling. *Nat. Chem. Biol.* **9**, 247–249

11. Lauth, M., Bergstrom, A., Shimokawa, T., and Toftgard, R. (2007) Inhibition of GLI-mediated transcription and tumor cell growth by small-molecule antagonists. *Proc. Natl. Acad. Sci. U. S. A.* **104**, 8455–8460

12. Rodgers, U. R., Lanyon-Hogg, T., Masumoto, N., Ritzefeld, M., Burke, R., Blagg, J., *et al.* (2016) Characterization of Hedgehog acyltransferase inhibitors identifies a small molecule probe for Hedgehog signaling by cancer cells. *ACS Chem. Biol.* **11**, 3256–3262

13. Yauch, R. L., Dijkgraaf, G. J., Alicke, B., Januario, T., Ahn, C. P., Holcomb, T., *et al.* (2009) Smoothened mutation confers resistance to a Hedgehog pathway inhibitor in medulloblastoma. *Science* **326**, 572–574

14. Dijkgraaf, G. J., Alicke, B., Weinmann, L., Januario, T., West, K., Modrusan, Z., *et al.* (2011) Small molecule inhibition of GDC-0449 refractory smoothened mutants and downstream mechanisms of drug resistance. *Cancer Res.* **71**, 435–444

15. Robinson, G. W., Orr, B. A., Wu, G., Gururangan, S., Lin, T., Qaddoumi, I., *et al.* (2015) Vismodegib exerts targeted efficacy against recurrent Sonic Hedgehog-Subgroup medulloblastoma: results from phase II pediatric brain tumor consortium studies PBTC-025B and PBTC-032. *J. Clin. Oncol.* **33**, 2646–2654

16. Belloni, E., Muenke, M., Roessler, E., Traverso, G., Siegel-Bartelt, J., Frumkin, A., *et al.* (1996) Identification of Sonic Hedgehog as a candidate gene responsible for holoprosencephaly. *Nat. Genet.* **14**, 353–356

17. Bumcrot, D. A., Takada, R., and McMahon, A. P. (1995) Proteolytic processing yields two secreted forms of Sonic Hedgehog. *Mol. Cell Biol.* **15**, 2294–2303

18. Porter, J. A., Young, K. E., and Beachy, P. A. (1996) Cholesterol modification of Hedgehog signaling proteins in animal development. *Science* **274**, 255–259

19. Callahan, B. P., and Wang, C. (2015) Hedgehog cholesterolysis: specialized gatekeeper to oncogenic signaling. *Cancers (Basel)* **7**, 2037–2053

20. Hall, T. M., Porter, J. A., Young, K. E., Koonin, E. V., Beachy, P. A., and Leahy, D. J. (1997) Crystal structure of a hedgehog autoprocessing domain: homology between hedgehog and self-splicing proteins. *Cell* **91**, 85–97

21. Perler, F. B. (1998) Protein splicing of inteins and Hedgehog autoproteolysis: structure, function, and evolution. *Cell* **92**, 1–4

22. Xie, J., Owen, T., Xia, K., Callahan, B., and Wang, C. (2016) A single aspartate coordinates two catalytic steps in hedgehog autoprocessing. *J. Am. Chem. Soc.* **138**, 10806–10809

23. Chen, X., Tukachinsky, H., Huang, C. H., Jao, C., Chu, Y. R., Tang, H. Y., *et al.* (2011) Processing and turnover of the Hedgehog protein in the endoplasmic reticulum. *J. Cell Biol.* **192**, 825–838

24. Huang, C. H., Hsiao, H. T., Chu, Y. R., Ye, Y., and Chen, X. (2013) Derlin2 protein facilitates HRD1-mediated retro-translocation of Sonic Hedgehog at the endoplasmic reticulum. *J. Biol. Chem.* **288**, 25330–25339

25. Tang, H. Y., Huang, C. H., Zhuang, Y. H., Christianson, J. C., and Chen, X. (2014) EDEM2 and OS-9 are required for ER-associated degradation of non-glycosylated Sonic Hedgehog. *PLoS One* **9**, e92164

26. Ciulla, D. A., Jorgensen, M. T., Giner, J. L., and Callahan, B. P. (2018) Chemical bypass of general base catalysis in Hedgehog protein cholesterolysis using a hyper-nucleophilic substrate. *J. Am. Chem. Soc.* **140**, 916–918

27. Amakye, D., Jagani, Z., and Dorsch, M. (2013) Unraveling the therapeutic potential of the Hedgehog pathway in cancer. *Nat. Med.* **19**, 1410–1422

28. Hall, M. P., Unch, J., Binkowski, B. F., Valley, M. P., Butler, B. L., Wood, M. G., *et al.* (2012) Engineered luciferase reporter from a deep sea shrimp utilizing a novel imidazopyrazinone substrate. *ACS Chem. Biol.* **7**, 1848–1857

29. Vincent, S., Thomas, A., Brasher, B., and Benson, J. D. (2003) Targeting of proteins to membranes through Hedgehog auto-processing. *Nat. Biotechnol.* **21**, 936–940

30. Mozhdehi, D., Luginbuhl, K. M., Dzuricky, M., Costa, S. A., Xiong, S., Huang, F. C., *et al.* (2019) Genetically encoded cholesterol-modified polypeptides. *J. Am. Chem. Soc.* **141**, 945–951

31. Traiffort, E., Dubourg, C., Faure, H., Rognan, D., Odent, S., Durou, M. R., *et al.* (2004) Functional characterization of Sonic Hedgehog mutations associated with holoprosencephaly. *J. Biol. Chem.* **279**, 42889–42897

32. Cooper, M. K., Porter, J. A., Young, K. E., and Beachy, P. A. (1998) Teratogen-mediated inhibition of target tissue response to Shh signaling. *Science* **280**, 1603–1607

33. Qiao, Y., Molina, H., Pandey, A., Zhang, J., and Cole, P. A. (2006) Chemical rescue of a mutant enzyme in living cells. *Science* **311**, 1293–1297

34. Lowry, W. E., Huang, J., Ma, Y. C., Ali, S., Wang, D., Williams, D. M., *et al.* (2002) Csk, a critical link of g protein signals to actin cytoskeletal reorganization. *Dev. Cell* **2**, 733–744

35. Marletta, M. A. (2006) Raising enzymes from the dead and the secrets they can tell. *ACS Chem. Biol.* **1**, 73–74

36. Inglese, J., Johnson, R. L., Simeonov, A., Xia, M., Zheng, W., Austin, C. P., *et al.* (2007) High-throughput screening assays for the identification of chemical probes. *Nat. Chem. Biol.* **3**, 466–479

37. He, X., Tan, C., Wang, F., Wang, Y., Zhou, R., Cui, D., *et al.* (2016) Knock-in of large reporter genes in human cells via CRISPR/Cas9-induced homology-dependent and independent DNA repair. *Nucleic Acids Res.* **44**, e85

38. Iannotti, M. J., MacArthur, R., Jones, R., Tao, D., Singec, I., Michael, S., *et al.* (2019) Detecting secretory proteins by acoustic droplet ejection in multiplexed high-throughput applications. *ACS Chem. Biol.* **14**, 497–505

39. Lindberg, E., Mizukami, S., Ibata, K., Fukano, T., Miyawakide, A., and Kikuchi, K. (2013) Development of cell-impermeable coelenterazine derivatives. *Chem. Sci.* **4**, 4395–4400

40. Chang, D. T., Lopez, A., von Kessler, D. P., Chiang, C., Simandl, B. K., Zhao, R., *et al.* (1994) Products, genetic linkage and limb patterning activity of a murine Hedgehog gene. *Development* **120**, 3339–3353

ASBMB

41. Jiang, S. Q., and Paulus, H. (2010) A high-throughput, homogeneous, fluorescence polarization assay for inhibitors of Hedgehog protein autoprocessing. *J. Biomol. Screen* **15**, 1082–1087

42. Owen, T. S., Ngoje, G., Lageman, T. J., Bordeau, B. M., Belfort, M., and Callahan, B. P. (2015) Forster resonance energy transfer-based cholesterolysis assay identifies a novel Hedgehog inhibitor. *Anal Biochem.* **488**, 1–5

43. Inglese, J., Auld, D. S., Jadhav, A., Johnson, R. L., Simeonov, A., Yasgar, A., *et al.* (2006) Quantitative high-throughput screening: a titration-based approach that efficiently identifies biological activities in large chemical libraries. *Proc. Natl. Acad. Sci. U. S. A.* **103**, 11473–11478

44. Wagner, A. G., Stagnitta, R. T., Xu, Z., Pezzullo, J. L., Kandel, N., Giner, J. L., *et al.* (2021) Nanomolar, noncovalent antagonism of hedgehog cholesterolysis: exception to the "irreversibility rule" for protein autoprocessing inhibition. *Biochemistry* **61**, 1022–1028

45. Smith, C. J., Wagner, A. G., Stagnitta, R. T., Xu, Z., Pezzullo, J. L., Giner, J. L., *et al.* (2020) Subverting hedgehog protein autoprocessing by chemical induction of paracatalysis. *Biochemistry* **59**, 736–741

46. Xie, J., Owen, T., Xia, K., Singh, A. V., Tou, E., Li, L., *et al.* (2015) Zinc inhibits hedgehog autoprocessing: Linking zinc deficiency with hedgehog activation. *J. Biol. Chem.* **290**, 11591–11600

47. Owen, T. S., Xie, X. J., Laraway, B., Ngoje, G., Wang, C., and Callahan, B. P. (2015) Active site targeting of hedgehog precursor protein with phenylarsine oxide. *Chembiochem* **16**, 55–58

48. V, V., and V, G. (2015) Multicomponent synthesis of novel coelenterazine derivatives substituted at the C-3 position. *Tetrahedron* **71**, 8781–8785